Maximum Efficiency Average Current Controller Based on a Comprehensive Charge Rate Model for DCM Boost PFC Converter

Linkai Li, Wanyang Wang, Dian Lyu, Run Min, *Member, IEEE*, Qiaoling Tong, *Member, IEEE*, Han Peng, *Member, IEEE*, and Jinchong Yu

***Abstract*—This article investigates modeling and control approaches to optimize the efficiency and power factor for discontinuous conduction mode boost power factor correction converters. First, with detailed consideration of parasitics and GaN HEMT transients, the input and output charges of the converter are exactly derived, where the rate forms the comprehensive charge rate (CCR) model. Second, based on the CCR model, the overall efficiency is derived. Since the overall efficiency is only related to the input voltage, output voltage, and switching ON-time, an optimal ON-time is calculated to achieve the maximum efficiency. Furthermore, with the optimal ON-time, a maximum efficiency average current (MEAC) controller is proposed to regulate the input current while maintaining the maximum efficiency. With the predefined optimal ON-time, a switching cycle modulation method is adopted to regulate the input current as sinusoid, which improves the power factor to unity. Finally, effectiveness of the MEAC control strategy is verified by simulations and experiments. Compared with conventional constant ON-time control, it achieves an optimized efficiency and power factor over a large operation range.**

***Index Terms*—Current control, discontinuous conduction mode (DCM), efficiency, GaN HEMTs, power converter, power factor correction (PFC).**

I. Introduction

POWER conversion efficiency is very important in wireless power transfer systems, plug-in electric vehicles, photovoltaic systems, and power factor correction (PFC) converters, etc. [1]–[5]. For PFC converters, many literatures focus on improving the power factor and inductor current distortion [6]–[8], whereas the efficiency optimization is less studied. However, as new industrial requirements and standards for PFC applications emerge, the existing techniques are facing more and more challenges. Specifically, it is rather difficult to optimize the efficiency over a wide operation range while achieving high power factor and low current distortion.

Among many active PFC strategies, boost PFC converter is a well-known scheme. Similar to other switching mode power converters, the boost PFC converter has different operation modes, i.e., continuous conduction mode (CCM), critical conduction mode (CRM), and discontinuous conduction mode (DCM). Generally, CCM operation is suitable for heavy load and high power rating, whereas CRM and DCM operations are usually used in low and medium power applications [9], [10]. Comparatively, CRM and DCM operations eliminate the diode reverse recovery problem while the turn-ON loss of power switch can be reduced through valley switching (VS) or zero voltage switching (ZVS) [11], [12]. Based on boost converter, efficiency comparison between CCM and DCM is presented in [13]. Although DCM suffers from higher inductor loss and diode loss, it has lower switching loss. Therefore, in some low power applications, DCM operation can achieve higher overall efficiency than CCM [14]. Besides, DCM operation has preferable advantages of simple compensation, high bandwidth, and compact and low-cost inductor.

Generally, power loss in a converter is mainly induced by switching and conduction losses. The switching loss increases significantly with the switching frequency, and it consists turn-ON loss and turn-OFF loss. For DCM boost PFC converter, the turn-ON loss is relatively minor, whereas the turn-OFF loss and conduction loss dominate the overall efficiency. Although the efficiency of PFC converter can be improved by GaN HEMTs [15], few studies focus on optimizing the efficiency through control strategies. For PFC applications, variable ON-time control is widely used to improve the power factor and current distortion [16], [17]. Furthermore, to improve the efficiency and ripple, variable ON-time control is modified to tune the switching frequency in each half line cycle [18]. However, without sinusoid input current, this strategy sacrifices the power factor and current distortion. Besides, the optimization cannot maximize the efficiency, since it lacks in-depth analysis for the relationship between ON-time control and efficiency. To optimize the efficiency of a power converter, accurate modeling and analysis for different losses are consistently required [19], [20]. Both switching loss and conduction loss need to be comprehensively studied to carry out the optimization.

Manuscript received December 30, 2019; revised July 18, 2020; accepted September 16, 2020. Date of publication September 23, 2020; date of current version January 22, 2021. This work was supported by the National Natural Science Foundation of China under Grants 61701184, 51877075, and 62074067. Recommended for publication by Associate Editor D. Maksimovic. *(Corresponding author: Run Min.)*

Linkai Li, Wanyang Wang, Dian Lyu, Run Min, Qiaoling Tong, and Jinchong Yu are with the School of Optical and Electronic Information, Huazhong University of Science and Technology, Wuhan 430074, China (e-mail: lilinkai@hust.edu.cn; m201972305@hust.edu.cn; Lyudian@hust.edu.cn; minrun@hust.edu.cn; tongqiaoling@hust.edu.cn; hkyjc_ic@hust.edu.cn).

Han Peng is with the State Key Laboratory of Advanced Electromagnetic Engineering and Technology, School of Electrical and Electronic Engineering, Huazhong University of Science and Technology, Wuhan 430074, China (e-mail: pengh@hust.edu.cn).

Color versions of one or more of the figures in this article are available online at https://ieeexplore.ieee.org.

Digital Object Identifier 10.1109/TPEL.2020.3026239

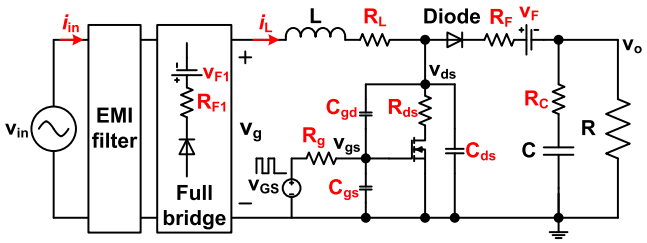

Fig. 1. Boost PFC converter with consideration of parasitics.

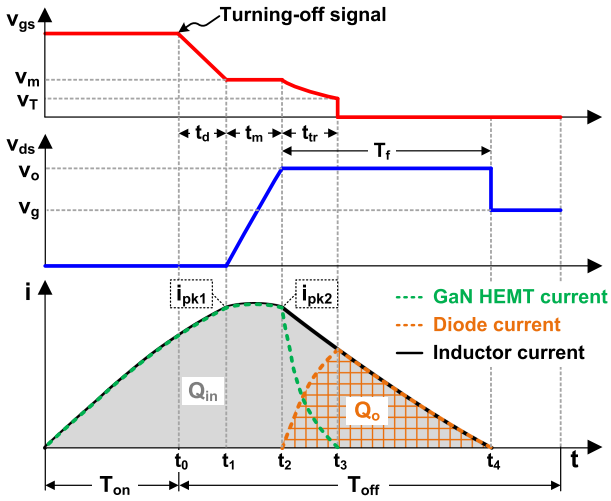

Fig. 2. Currents and voltages in boost PFC converter.

In this article, a comprehensive charge rate (CCR) model is proposed for boost PFC converter operating in DCM, where a GaN HEMT is used as main power switch. With consideration of parasitics and GaN HEMT dynamics, both the input and output charges are accurately calculated. This forms the CCR model, which is used to derive the overall efficiency under different input and output voltages. Furthermore, to maximize the efficiency and regulate the input current of boost PFC converter, a maximum efficiency average current (MEAC) controller is proposed. Combining the efficiency chart derived from the CCR model, this controller adaptively regulates the switching-ON time to achieve maximum efficiency under different inputs and outputs. While the switching-ON time is tuned to optimize the efficiency, a variable switching cycle is adopted to regulate the inductor current average value as sinusoid, which optimizes the power factor. Finally, simulations and experiments are given to verify accuracy of the proposed CCR model and effectiveness of MEAC controller.

The rest of this article is organized as follows. In Section II, the CCR model for DCM boost PFC converter is derived from the input and output charges. Section III gives out the MEAC control strategy and explicit efficiency analyses based on simulations. Furthermore, experimental results are given in Section IV to verify accuracy of the proposed CCR model and effectiveness of MEAC controller. Finally, the conclusion is given in Section V.

II. CCR Model for DCM Boost PFC Converter

DCM boost PFC converters are widely used in low power applications. When operating in DCM, the diode reverse recovery problem is eliminated. Besides, turn-ON loss of power switch can be reduced through the well-known VS or ZVS techniques. However, DCM operation usually suffers from higher conduction loss owning to the increased current ripple. Moreover, turn-OFF loss still exists since the inductor current is not zero when power switch is turned OFF. Both conduction loss and turn-OFF loss are induced by parasitics, which affect the efficiency of the converter.

In fact, the overall efficiency of the DCM converter in each switching cycle is determined by the input and output charges. Therefore, the CCR model is proposed in the followings, which is derived with consideration of parasitics and switching dynamics.

A boost PFC converter with consideration of parasitics is given in Fig. 1, where R_L is the equivalent series resistance of inductor, R_{ds} and R_g are the conduction and gate resistances of the GaN HEMT, respectively, R_F and v_F are forward resistance and voltage of the diode, respectively, and R_C is the equivalent series resistance of the capacitor. Parasitic capacitances of the GaN HEMT include C_{gs}, C_{gd}, and C_{ds}.

When the converter operates in DCM, dynamic states in the converter are given in Fig. 2. Analyses for different stages are given in the following.

1) 0–t_0: In this stage, the GaN HEMT is turned ON, and the turning-OFF driving signal occurs at time t_0.
2) t_0–t_1: This stage is called turn-OFF delay period. The driving current discharges C_{gs} until the driving voltage v_{gs} drops to a constant value v_m, which is caused by the well-known Miller effect. In this duration, the GaN HEMT is still turned ON. The inductor current rises until it reaches the peak current $i_{\rm pk1}$.
3) t_1–t_2: The driving voltage v_{gs} maintains at the Miller voltage v_m. Since v_{gs} has little change in this duration, a constant current flows through C_{gd}. This current is equal to v_m/R_g, and it charges C_{gd} until v_{ds} reaches the output voltage. Besides, the inductor current changes from $i_{\rm pk1}$ to $i_{\rm pk2}$, depending on the voltage-second product of the inductor.
4) t_2–t_3: In this stage, C_{gs} is discharged through R_g, and v_{gs} falls from v_m to the threshold voltage v_T. Owning to the decreasing overdrive voltage, the GaN HEMT current drops from $i_{\rm pk2}$ to zero, whereas the SiC diode current increases from zero to the inductor current.
5) t_3–t_4: The GaN HEMT is completely turned OFF in this stage, and the inductor current falls until it reaches zero.
6) t_4–: Both the GaN HEMT and diode are OFF, and v_{ds} drops to v_g.

In the followings, the inductor current is exactly calculated for different stages with consideration of the switching transition. Based on the current expressions, the input and output charges are derived. Furthermore, expressions for the overall efficiency and power loss are acquired.

A. Inductor Current During Switching-ON

When the main switch is ON, voltage on the inductor equals $|v_{\rm in}| - 2v_{F1} - (R_L + R_{ds} + 2R_{F1})i_L(t)$, where $i_L(t)$ denotes the inductor current. Therefore, differential equation of $i_L(t)$ is

given by

$$\begin{cases} L\frac{di_L(t)}{dt} = v_g - R_{\text{eq,on}} i_L(t) \\ i_L(0) = 0 \end{cases} \quad \text{s.t. } t \le t_1 \tag{1}$$

where $v_g = |v_{\text{in}}| - 2v_{F1}$ and $R_{\text{eq,on}} = R_L + R_{ds} + 2R_{F1}$. Furthermore, $i_L(t)$ is derived as

$$i_L(t) = \frac{v_g}{R_{\text{eq,on}}}(1 - e^{-\frac{R_{\text{eq,on}}}{L}t}) \text{ s.t. } t \le t_1. \tag{2}$$

Substituting $t = t_1 = T_{\text{on}} + t_d$ into (2) gives

$$i_{\text{pk1}} = \frac{v_g}{R_{\text{eq,on}}}(1 - e^{-R_{\text{eq,on}}(T_{\text{on}}+t_d)/L}). \tag{3}$$

At time t_0, the driving signal v_{GS} drops to zero. However, the GaN HEMT is not turned OFF instantly owing to the turn-OFF delay and Miller effect.

B. GaN HEMT Turn-Off Process

As shown in Fig. 2, the turn-OFF process of the GaN HEMT begins at time t_0 and ends at time t_3. Since the turn-OFF speed of GaN HEMTs is very fast, the driving voltage during GaN HEMTs turn-OFF can be considered as a linear change [21].

In the turn-OFF delay period, C_{gs} is discharged through R_g. The driving voltage drops from v_{gs} to v_m, and the turn-OFF delay time is given by

$$t_d = \frac{Q_{gs1} R_g}{(v_{gs} + v_m)\ 2} \tag{4}$$

where Q_{gs1} represents the corresponding charge during t_d.

During $t_1 < t < t_2$, v_{gs} equals the Miller voltage v_m, which is nearly constant owing to the Miller effect. Therefore, a constant driving current v_m/R_g charges C_{gd}, which makes v_{ds} rise from zero to v_o. When v_{ds} rises from zero to v_o, the time duration is given by

$$t_m = \frac{Q_{gd} R_g}{v_m} \tag{5}$$

where Q_{gd} represents the corresponding charge during t_m.

In this duration, the GaN HEMT is saturated, and the drain-source current can be approximated by the same as MOSFET [22]

$$i_{ds} = \beta(v_{gs} - v_T)^2(1 + \lambda v_{ds}) \tag{6}$$

where β and λ are constant. At time $t = t_2$, the current equals i_{pk2} while v_{ds} rises to v_o. Since voltage-second product of the inductor is given by $(v_g - v_o/2)t_m$, the current at $t = t_2$ is given by

$$i_{\text{pk2}} = i_{\text{pk1}} + \frac{(v_g - v_o/2)t_m}{L}. \tag{7}$$

At time t_2, C_{gd} is fully charged, and v_{ds} stops rising. After t_2, the GaN HEMT current begins to fall.

During $t_2 < t < t_3$, the inductor current is transmitted from the GaN HEMT to the diode. In this duration, the driving voltage v_{gs} drops from v_m to v_T since C_{gs} is discharged through R_g. Furthermore, the time duration and v_{gs} are given by (8), where variation of v_{gs} is seen as linear. This approximation is valid in most applications with GaN HEMT, since $v_m - v_T$ is very small

$$\begin{cases} t_{tr} = t_3 - t_2 = \frac{Q_{gs2} R_g}{(v_m + v_T)\ 2} \\ v_{gs} \approx v_m - \frac{v_m - v_T}{t_{tr}} t \end{cases} \tag{8}$$

where Q_{gs2} represents the corresponding charge during t_{tr}.

Substituting (8) into (6) gives the GaN HEMT current

$$\begin{aligned} i_{ds} &= \beta\left(\frac{t}{t_{tr}} - 1\right)^2 (v_T - v_m)^2(1 + \lambda v_{ds}) \\ &= \left(\frac{t}{t_{tr}} - 1\right)^2 i_{\text{pk2}}. \end{aligned} \tag{9}$$

After $t = t_3$, the GaN HEMT is completely turned OFF, and the inductor current flows to the output through the diode.

C. Inductor Current During Switching-OFF

During $t_2 < t < t_4$, voltage on the inductor is $|v_{\text{in}}| - 2v_{F1} - v_F - v_o - (R_L + R_F + 2R_{F1})i_L(t)$. Therefore, differential equation of $i_L(t)$ is given by

$$\begin{cases} L\frac{di_L(t)}{dt} = v_{\text{eq,off}} - R_{\text{eq,off}} i_L(t) \\ i_L(t_2) = i_{\text{pk2}} \end{cases} \quad \text{s.t. } t_2 < t \le t_4 \tag{10}$$

where $v_{\text{eq,off}} = v_g - v_F - v_o$ and $R_{\text{eq,off}} = R_L + R_F + 2R_{F1}$. Furthermore, $i_L(t)$ is given by

$$\begin{aligned} i_L(t) = \frac{v_{\text{eq,off}}}{R_{\text{eq,off}}} + \left(i_{\text{pk2}} - \frac{v_{\text{eq,off}}}{R_{\text{eq,off}}}\right) \\ \times e^{-\frac{R_{\text{eq,off}}}{L}(t - t_2)} \text{ s.t. } t_2 < t \le t_4. \end{aligned} \tag{11}$$

At time $t = t_4$, the current falls to zero. Therefore, substituting $i_L(t_4) = 0$ into (11) derives the duration

$$T_f = t_4 - t_2 = \frac{L}{R_{\text{eq,off}}} \ln\left(1 - \frac{i_{\text{pk2}} R_{\text{eq,off}}}{v_{\text{eq,off}}}\right). \tag{12}$$

Based on the exact inductor current model, the input and output charges are calculated in the following.

D. CCR Model and Overall Efficiency of the Converter

In the followings, overall efficiency of the converter is derived from the CCR model, which is the rate between the total input and output charges. The input charge is determined by integration of $i_L(t)$ during $0 < t < t_4$, as shown in the following:

$$\begin{aligned} Q_{\text{in}} &= \int_0^{t_4} i_L(t)dt \\ &\approx \int_0^{t_1} i_L(t)dt + \int_{t_2}^{t_4} i_L(t)dt + \frac{(i_{pk1} + i_{pk2})t_m}{2}. \end{aligned} \tag{13}$$

In order to solve the equation, (1) and (10) are integrated, respectively. The results are given by

$$\begin{cases} \int_0^{t_1} i_L(t)dt = \frac{v_g(T_{\text{on}} + t_d) - i_{\text{pk1}} L}{R_{\text{eq,on}}} \\ \int_{t_2}^{t_4} i_L(t)dt = \frac{v_{\text{eq,off}} T_f + L i_{\text{pk2}}}{R_{\text{eq,off}}}. \end{cases} \tag{14}$$

Furthermore, substituting (14) into (13) gives the input charge

$$\begin{aligned} Q_{\text{in}} = \frac{v_g\,(T_{\text{on}} + t_d) - i_{\text{pk1}} L}{R_{\text{eq,on}}} + \frac{v_{\text{eq,off}} T_f + L i_{\text{pk2}}}{R_{\text{eq,off}}} \\ + \frac{(i_{\text{pk1}} + i_{\text{pk2}})t_m}{2}. \end{aligned} \tag{15}$$

The output charge is determined by the diode current, and it is given by

$$Q_{\text{out}} = \int_{t_2}^{t_4} i_L(t)dt - Q_d \tag{16}$$

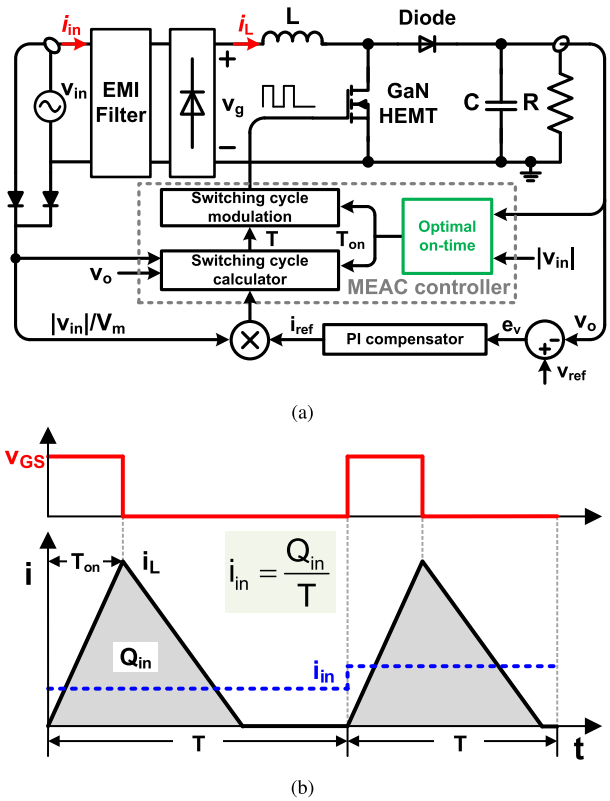

Fig. 3. DCM boost PFC converter with MEAC control. (a) Control scheme. (b) Switching cycle modulation.

where Q_d is the charge that flows through the GaN HEMT during $t_2 < t < t_3$. Based on (9), the charge is given by

$$Q_d = i_{\mathrm{pk2}} \int_0^{t_{tr}} \left(\frac{t}{t_{tr}} - 1 \right)^2 dt = \frac{i_{\mathrm{pk2}} t_{tr}}{3}. \tag{17}$$

Finally, overall efficiency of the converter is derived with the input charge, output charge, and T_{on} through the CCR model, which is shown in (18), at the bottom of this page. Besides, the energy loss is given by

$$W_{\mathrm{loss}} = W_{\mathrm{in}} - W_{\mathrm{out}}. \tag{19}$$

Both η and W_{loss} are functions of $\{v_o, |v_{\mathrm{in}}|, T_{\mathrm{on}}\}$. Since $|v_{\mathrm{in}}|$ and v_o may change a lot in applications, T_{on} can be adaptively tuned to maximize the efficiency.

III. MEAC Control for DCM Boost PFC Converter

Based on the CCR model, the MEAC control strategy is proposed to optimize the efficiency and to achieve average current control. Scheme of a DCM boost PFC converter with the proposed control strategy is given in Fig. 3(a). Since overall power loss and efficiency are functions of $\{v_o, |v_{\mathrm{in}}|, T_{\mathrm{on}}\}$, a suitable T_{on} is acquired through $|v_{\mathrm{in}}|$ and v_o. Furthermore, switching cycle modulation is used to generate the pulse signal that drives the GaN HEMT. The PI compensator is used to compensate the loop, which improves the stability and eliminates steady-state error in output voltage.

As shown in Fig. 3(b), the switching cycle is calculated and modulated so that the input current is regulated as $i_{\mathrm{ref}} \sin(\varphi)$. Similar to the conventional digital pulsewidth modulation, the switching cycle modulation adopts a counter and comparator to carry out modulation. The counter signal rises until it reaches T, and it is compared to T_{on} to generate the pulse signal. Average current control is realized by tuning the switching cycle according to the input charge.

TABLE I
SPECIFICATIONS OF THE PROTOTYPE

Input voltage v_{in}	165 VAC $\sim$ 235 VAC / 50 Hz
Switching frequency f_s	20 kHz $\sim$ 300 kHz for constant on-time control, 34 kHz $\sim$ 420 kHz for MEAC control
PI gains	$k_P = 1.1$, $k_I = 32$
Sample gain	$k_{sample} = 0.0088$
Output voltage v_o	390 V
Maximum power rating	310 W
Boost inductor	$L = 20$ μH, $R_L = 200$ mΩ
Output capacitor	$C = 68$ μF, $R_C = 30$ mΩ
GaN HEMT	$R_g = 5$ Ω, $R_{ds} = 50$ mΩ, $Q_{gs1} = 2.2$ nC, $Q_{gd} = 1.8$ nC, $Q_{gs2} = 1.8$ nC, $v_T = 1.5$ V, $v_m = 3$ V
SiC diode	$v_F = 1.56$ V, $R_F = 200$ mΩ
Rectifier bridge	$v_{F1} = 0.98$ V, $R_{F1} = 100$ mΩ
Driving voltage	5.6 V

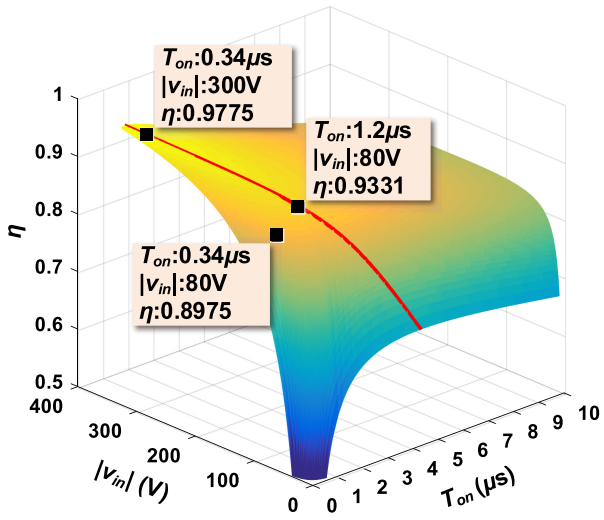

Fig. 4. Variation of efficiency with $|v_{\mathrm{in}}|$ and T_{on} when $v_o = 400$ V.

A. Maximum Efficiency Point

Based on (18) and specifications in Table I, the efficiency is simulated under different conditions. At nominal output, the efficiency is plotted in Fig. 4.

$$\eta = f(v_o, |v_{\mathrm{in}}|, T_{\mathrm{on}}) = \frac{W_{\mathrm{out}}}{W_{\mathrm{in}}} = \frac{v_o}{|v_{\mathrm{in}}|} \frac{v_{\mathrm{eq,off}} T_f + i_{\mathrm{pk2}} L - t_{tr} i_{\mathrm{pk2}} R_{\mathrm{eq,off}}/3}{[v_g (T_{\mathrm{on}} + t_d) - i_{\mathrm{pk1}} L] R_{\mathrm{eq,off}}/R_{\mathrm{eq,on}} + v_{\mathrm{eq,off}} T_f + i_{\mathrm{pk1}} L + R_{\mathrm{eq,off}} (i_{\mathrm{pk1}} + i_{\mathrm{pk2}}) t_m/2} \tag{18}$$

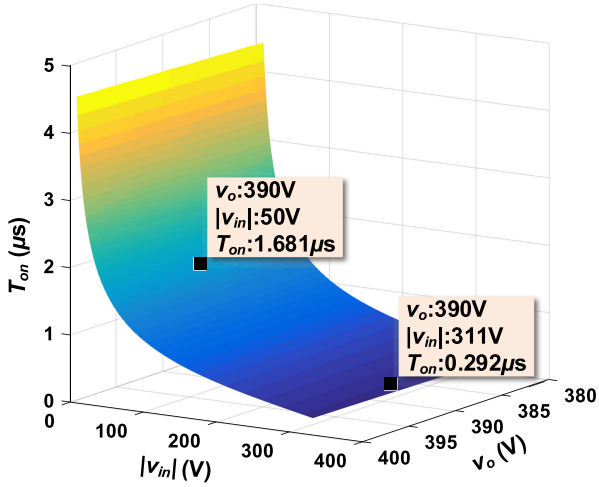

Fig. 5. Optimal $T_{\rm on}$ with different $|v_{\rm in}|$ and v_o.

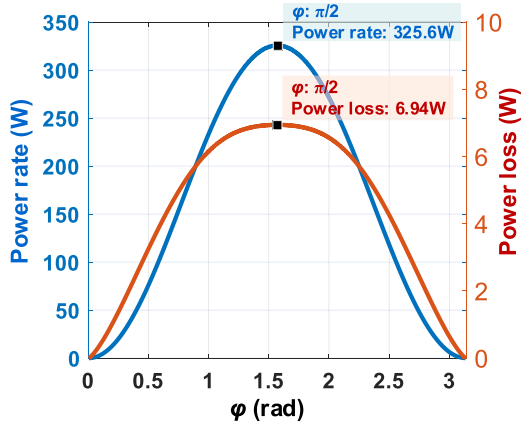

Fig. 6. Power rate and power loss with respect to the phase angle.

The efficiency is influenced by $T_{\rm on}$, and it increases along with $|v_{\rm in}|$. Besides, for each level of input voltage, there is a maximum efficiency point, which can be achieved by a specific $T_{\rm on}$. When $|v_{\rm in}| = 300$ V, the maximum efficiency is 97.75%, where $T_{\rm on}$ equals 0.34 μs. With the same $T_{\rm on}$, the efficiency drops to 89.75% when $|v_{\rm in}| = 80$ V. For $|v_{\rm in}| = 80$ V, the efficiency can be improved to 93.31% by setting $T_{\rm on}$=1.2 μs.

In PFC applications, the input voltage varies a lot in each half line cycle, which greatly influence the efficiency. Therefore, $T_{\rm on}$ can be adaptively tuned to maximize the efficiency. The optimal $T_{\rm on}$ with different $|v_{\rm in}|$ and v_o is plotted in Fig. 5.

When v_o=390 V and $|v_{\rm in}|$=311 V, the optimal $T_{\rm on}$ is 0.292 μs. When v_o=390 V and $|v_{\rm in}|$=50 V, the optimal $T_{\rm on}$ increases to 1.681 μs. Since the optimal $T_{\rm on}$ may change a lot in each half line cycle, the MEAC control strategy is proposed to maximize the efficiency while to achieve average current control.

B. MEAC Control

For DCM boost PFC converter, the input current average value can be regulated through switching cycle modulation. Based on the input charge, the input current is given by

$$i_{\rm in} = \frac{1}{T}\left[\frac{v_g(T_{\rm on}+t_d)-i_{\rm pk1}L}{R_{\rm eq,on}} + \frac{v_{\rm eq,off}T_f + Li_{\rm pk2}}{R_{\rm eq,off}} + \frac{(i_{\rm pk1}+i_{\rm pk2})t_m}{2}\right]. \tag{20}$$

In order to simplify the controller, parasitics are neglected in calculating the input current, and it gives

$$i_{\rm in} \approx \frac{1}{T}\frac{{T_{\rm on}}^2 v_{\rm in} v_o}{2(v_o-|v_{\rm in}|)L}. \tag{21}$$

In order to improve the power factor, magnitude of input current should be regulated to track the reference current. Therefore, substituting $i_{\rm in} = i_{\rm ref}\sin(\varphi)$ into (21) gives the switching cycle

$$T = \frac{1}{i_{\rm ref}\sin(\varphi)}\frac{{T_{\rm on}}^2 V_m \sin(\varphi) v_o}{2(v_o-|v_{\rm in}|)L} = \frac{{T_{\rm on}}^2 V_m v_o}{2i_{\rm ref}(v_o-|v_{\rm in}|)L}. \tag{22}$$

Based on (22), the input current is regulated as $i_{\rm in} = i_{\rm ref}\sin(\varphi)$ through modulating the switching cycle, and this optimizes the power factor.

C. Efficiency Over a Half Line Cycle

In PFC applications, the input voltage varies from zero to its peak value V_m in each half line cycle, as shown in the following:

$$v_{\rm in}(\varphi) = V_m \sin(\varphi) \tag{23}$$

where φ is the line angle. Based on MEAC controller, both $T_{\rm on}$ and T are adaptively tuned to ensure maximum efficiency while to achieve average current control. The input current is regulated as (24) to improve the power factor

$$i_{\rm in}(\varphi) = I_m \sin(\varphi). \tag{24}$$

Substituting (24) into (22) gives the switching cycle with respect to φ, as shown in the following:

$$T(\varphi) = \frac{1}{2LI_m}\frac{{T_{\rm on}}^2 V_m v_o}{v_o - V_m\sin(\varphi)}. \tag{25}$$

Furthermore, the input and output power rates are given by

$$\begin{cases} P_{\rm in}(\varphi) = \frac{Q_{\rm in}(\varphi)v_{\rm in}(\varphi)}{T(\varphi)} \\ P_{\rm out}(\varphi) = \frac{Q_{\rm out}(\varphi)v_o}{T(\varphi)}. \end{cases} \tag{26}$$

Finally, the efficiency over a half line cycle is given by

$$\eta_{\rm HLC} = \frac{\int_0^\pi P_{\rm out}(\varphi)d\varphi}{\int_0^\pi P_{\rm in}(\varphi)d\varphi}. \tag{27}$$

Based on specifications in Table I, the input power rate and power loss in a half line cycle are plotted in Fig. 6.

Both power rate and power loss reach their peak value when $\varphi = \pi/2$, where $v_{\rm in}(\varphi) = V_m$. The maximum power rate is 325.6 W, whereas the maximum power loss is 6.94 W. As the phase angle increases or decreases, both power rate and power loss decline. However, since the power rate declines by a faster rate than the power loss, the efficiency is degraded.

Furthermore, although the efficiency is optimized by tuning $T_{\rm on}$, it still decreases heavily when $|\varphi - \pi/2|$ is too high, as indicated in Fig. 7.

When $\varphi = \pi/2$, the efficiency reaches its peak value as 97.87% while $T_{\rm on}$ is the lowest, i.e., 0.292 μs. As the phase angle increases or decreases, $T_{\rm on}$ is enlarged adaptively, whereas the efficiency is still degraded. The efficiency is lower than 90% when $\varphi < 0.145$ or $\varphi > 2.995$. This indicates that the efficiency cannot achieve 90% when $v_{\rm in}(\varphi) < 45$ V, no matter how $T_{\rm on}$ is tuned. In order to avoid power loss in this condition, the whole

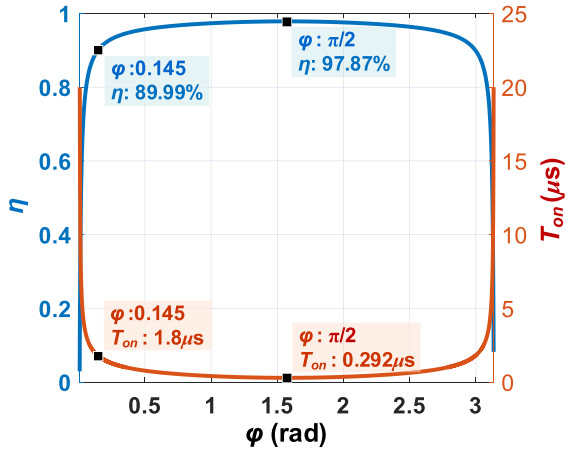

Fig. 7. Efficiency and optimal $T_{\rm on}$ with respect to the phase angle.

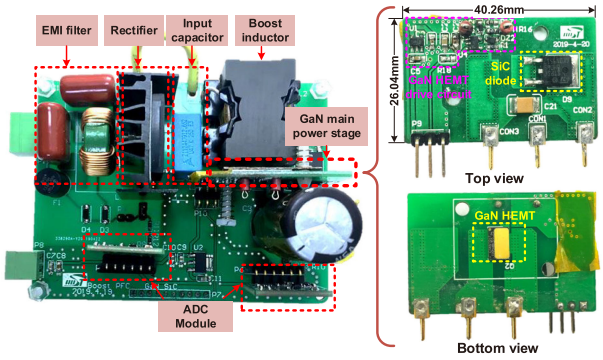

Fig. 8. Photograph of the prototype.

converter can be shut down to improve the overall efficiency in a half line cycle.

IV. Experiments

A boost PFC converter operating in DCM is constructed for experiments, as shown in Fig. 8. All control algorithms are implemented through an FPGA board (Altera Cyclone IV).

The ac line voltage is rectified by a 600 V/6 A rectifier bridge GBU6J from ON Semiconductor after the electromagnetic interference filter. A 470-nF input filter capacitor behind the rectifier bridge is used to filter switching harmonic. The 650 V/30 A GaN HEMT GS66508T from GaN Systems and SiC diode STPSC8H065B from STMicroelectronics are used for power switch and boost diode, respectively. The GaN HEMT is driven by the UCC27517 driver chip. A 68-μF capacitor (NFA500VB68M) and a 0.1-μF bypass capacitor are adopted as the output capacitor. The core and bobbin of boost inductor are PQ26/20. Line and output voltages are sampled by two single-channel 14-b A/D converter chips (LTC2314). To improve the transient response while reducing the ripple in $i_{\rm ref}$, the PI gains are set as $k_P = 1.1$ and $k_I = 32$. Detailed parameter values of the components are given in Table I.

In the following, accuracy of the proposed CCR model is verified through comparison between the model and the measured results. Furthermore, the efficiency under MEAC controller is compared to that of a fixed $T_{\rm on}$ controller, which also adopts variable switching cycle to carry out average current control.

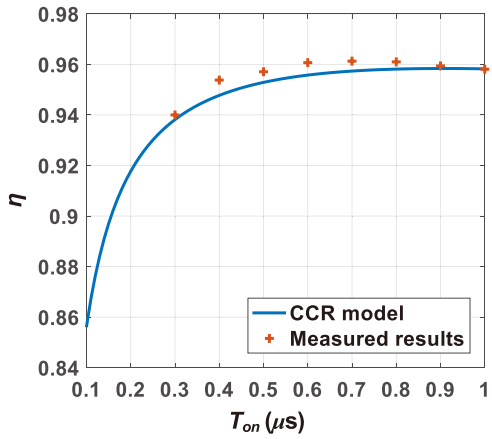

Fig. 9. Comparison between the CCR model and the measured results.

A. Verification of the CCR Model

Based on (18) and (27), the efficiency is estimated by the proposed model in different operation conditions. Accuracy of the CCR model is verified by comparison with the measured efficiency in a half line cycle, as shown in Fig. 9.

The comparison is given under the condition $v_{\rm in} = 220$ Vac, $v_o = 390$ V, and load resistance $R = 1000\ \Omega$. In experimental verification, the efficiency in a half line cycle is measured using the power analyzer PA5000H. As the results show, the efficiency calculated by the CCR model increases first with the increase of $T_{\rm on}$, and then gradually flattens. The CCR model highly matches with that of the measured results.

B. Nominal Inductor Current and Output Voltage Ripple

Nominal inductor current, input current and output voltage ripple are measured under MEAC control and constant ON-time control, respectively. The switching ON-time is set as 0.9 μs for constant ON-time control. According to analyses in Section III, the efficiency cannot achieve 90% when input voltage is lower than 45 V. Therefore, the PFC converter is shut down when the input voltage is below 50 V in the experiment. The measured inductor currents in a line cycle are given in Figs. 10 and 11.

For 165- and 220-Vac inputs, the inductor current peak value within a line cycle is 6.4 A under MEAC control, and it increases to 11 and 17.5 A under constant ON-time control, respectively.

As shown in Figs. 12 and 13, input currents under both controls are regulated as near sinusoid, which improves the power factor. For MEAC control, the converter is shut down when the input voltage is below 50 V. With 165- and 220-Vac inputs, the power factors under constant ON-time control are 0.996 and 0.983, respectively. While the power factors under MEAC control are 0.995 and 0.990, respectively.

Furthermore, the output voltage ripple is also measured, as shown in Figs. 14 and 15. With 165-Vac input, the voltage ripple under MEAC control is 22 V, whereas the ripple under constant ON-time control is 24 V. Therefore, the voltage ripple is reduced by 8.3% under MEAC control. Furthermore, when the input voltage is increased to 220 Vac, the voltage ripple under constant ON-time control is increased to 24.8 V, whereas it remains unchanged under MEAC control.

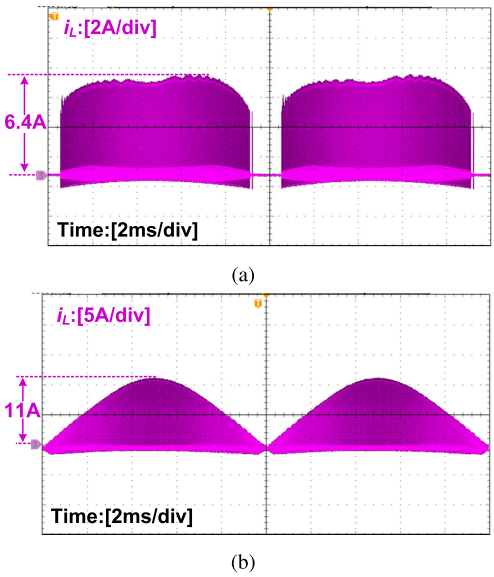

Fig. 10. Inductor current in a line cycle with 165-Vac input at 150-W output. (a) MEAC control. (b) Constant ON-time control.

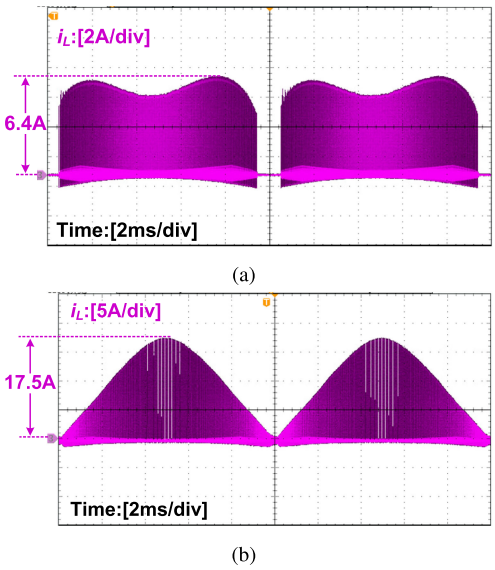

Fig. 11. Inductor current in a line cycle with 220-Vac input at 150-W output. (a) MEAC control. (b) Constant ON-time control.

C. Efficiency and Power Factor Under Different Operation Conditions

Efficiency of the converter is measured under different control strategies and operation conditions. The results of the proposed MEAC controller are compared with that of a constant ON-time controller. The measured efficiencies under different input voltages at 150-W output are plotted in Fig. 16.

As the measured results show, efficiency under MEAC controller is always the highest among other controllers. For constant ON-time control, the efficiency is highly dependent on $T_{\rm on}$, which is difficult to optimize. Although the efficiency under $T_{\rm on} = 0.9\,\mu$s is higher than that under $T_{\rm on} = 0.4\,\mu$s, it is still lower than that under MEAC control. For example, with

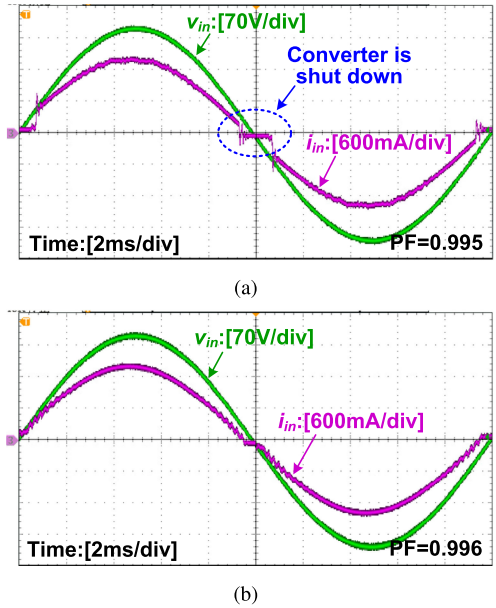

Fig. 12. Input current and input voltage in a line cycle with 165-Vac input at 150-W output. (a) MEAC control. (b) Constant ON-time control.

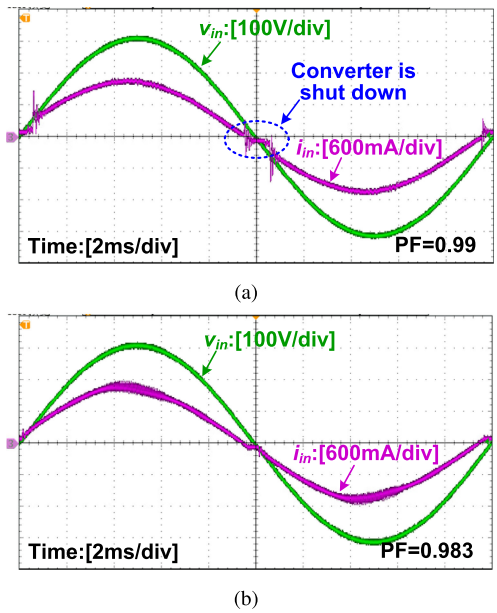

Fig. 13. Input current and input voltage in a line cycle with 220-Vac input at 150-W output. (a) MEAC control. (b) Constant ON-time control.

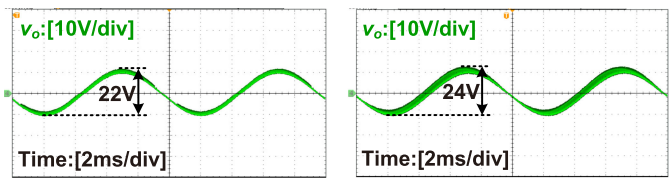

Fig. 14. Output voltage ripple in a line cycle with 165-Vac input at 150-W output. (a) MEAC control. (b) Constant ON-time control.

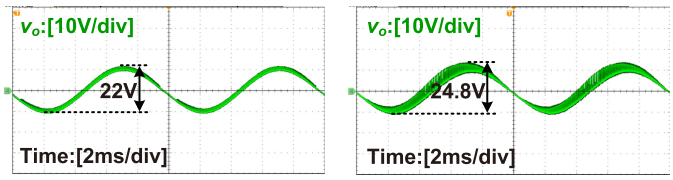

(a) (b)

Fig. 15. Output voltage ripple in a line cycle with 220-Vac input at 150-W output. (a) MEAC control. (b) Constant ON-time control.

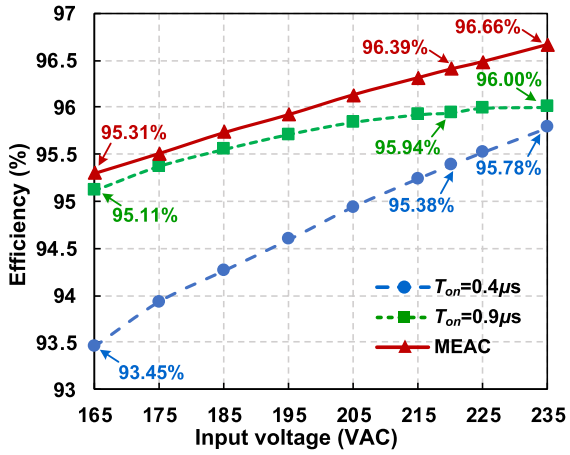

Fig. 16. Measured efficiency under different control strategies at 150-W output.

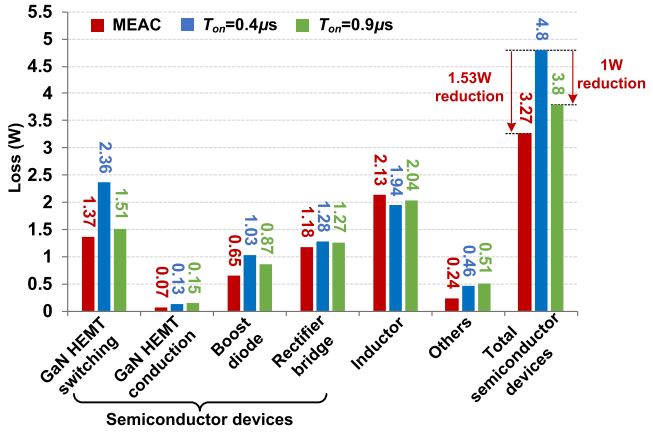

Fig. 17. Loss breakdown with 220-VAC input at 150-W output under different control strategies.

235-Vac input, a constant ON-time of 0.9 μs achieves an efficiency of 96.00%, which is 0.66% lower than that of MEAC controller. According to the tested results in Fig. 16, the MEAC controller improves the overall efficiency by an average of 0.78%.

With 220-Vac input, the loss breakdown under different control strategies is shown in Fig. 17. Compared with the constant ON-time control under $T_{\rm on}=0.4\,\mu$s, the total losses of semiconductor devices are reduced by 1 W under $T_{\rm on}=0.9\,\mu$s. The total losses of semiconductor devices under MEAC controller are lowest among other controllers, which results in the highest efficiency of 96.39%.

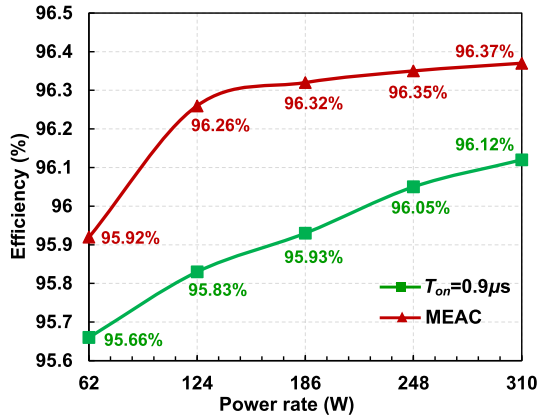

Fig. 18. Measured efficiency with MEAC and constant ON-time controls under different power rates.

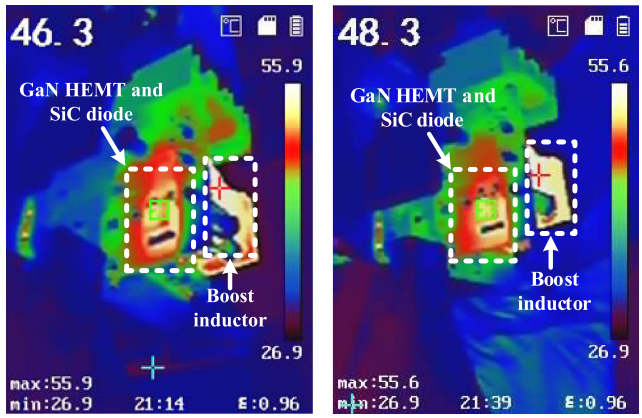

(a) (b)

Fig. 19. Infrared photographs under different control strategies at 150-W output. (a) MEAC control. (b) Constant ON-time control under $T_{\rm on}=0.9\,\mu$s.

Furthermore, comparisons are also given under different power rate, as shown in Fig. 18. The efficiency under MEAC control is compared with that of constant ON-time control with $T_{\rm on}=0.9\,\mu$s ($T_{\rm on}=0.9\,\mu$s achieves the highest efficiency under constant ON-time control). Compared with constant ON-time control, the MEAC control can achieve a higher efficiency within the entire load range.

Since MEAC control achieves higher efficiency than that of constant ON-time control, the temperature is improved. Infrared photos for converters under MEAC control and constant ON-time control are given in Fig. 19.

As the infrared photographs show, the maximum temperature under both controls occurs at the boost inductor. The maximum temperature under MEAC control achieves 55.9 °C, which is slightly higher than that of constant ON-time control. But, the temperature of main power stage under MEAC control is 46.3 °C, which is 2 °C lower than that of constant ON-time control.

The measured power factor and total harmonic distortion (THD) under different control strategies and operation conditions are given in Figs. 20 and 21. Under constant ON-time control, $T_{\rm on}$ has considerable influence on both power factor and THD. When the input voltage is 165 Vac, a constant ON-time of

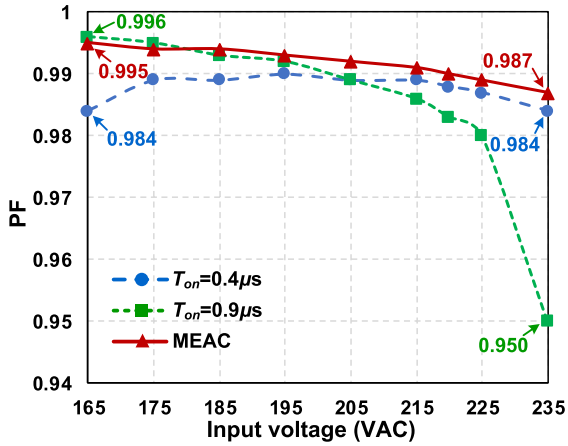

Fig. 20. Measured power factor under different control strategies at 150-W output.

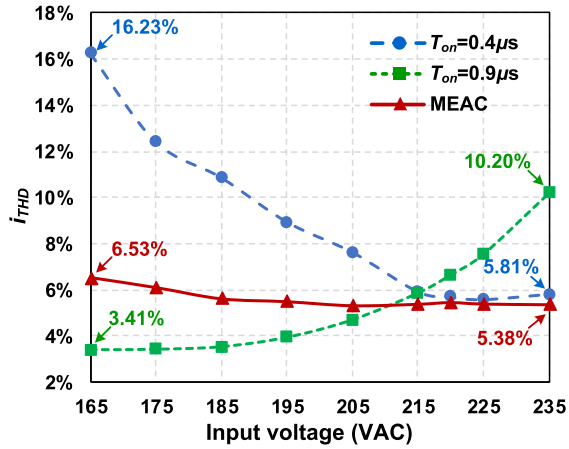

Fig. 21. Measured THD under different control strategies at 150-W output.

$T_{\rm on}=0.9$ μs achieves a power factor and THD of 0.996 and 3.41%, respectively. However, under $T_{\rm on}=0.4$ μs, the power factor and THD are degraded to 0.984 and 16.23%, respectively. Besides, as the input voltage increases to 235 Vac, the power factor and THD under $T_{\rm on}=0.9$ μs are degraded to 0.950 and 10.20%, respectively. In contrast, under MEAC control, variations of both power factor and THD with input voltage are significantly reduced.

D. Transient Performance

Fig. 22 gives the transient response under the MEAC control with 220-Vac input. The MEAC control strategies effectively stabilize the output voltage when the load steps. For 220-Vac input, when the load steps from 75 to 150 W and from 150 to 75 W, the response times are 80 and 160 ms, respectively. These experimental results verify that the proposed MEAC control can achieve a relatively fast response speed for PFC applications.

All experimental results prove analyses in Sections II and III. Effectiveness of the proposed MEAC control strategy is verified.

V. Conclusion

This article presents a CCR model and MEAC control strategy for DCM boost PFC converter. The CCR model is established through the input and output charges of the converter, which are calculated with consideration of parasitic resistances, capacitances, and GaN HEMT characteristics. Based on the CCR model, the overall efficiency is derived with changes of input voltage, output voltage, and switching ON-time. At each operation point, there is a specific switching ON-time that maximizes the efficiency. Therefore, the MEAC controller is proposed, which adapts the switching ON-time to maximizing the efficiency. Furthermore, the switching cycle is adjusted to regulate the input current as sinusoidal, which improves the power factor and THD. Experimental results show that the efficiency under MEAC controller is improved by an average of 0.78%, compared to that of constant ON-time controller.

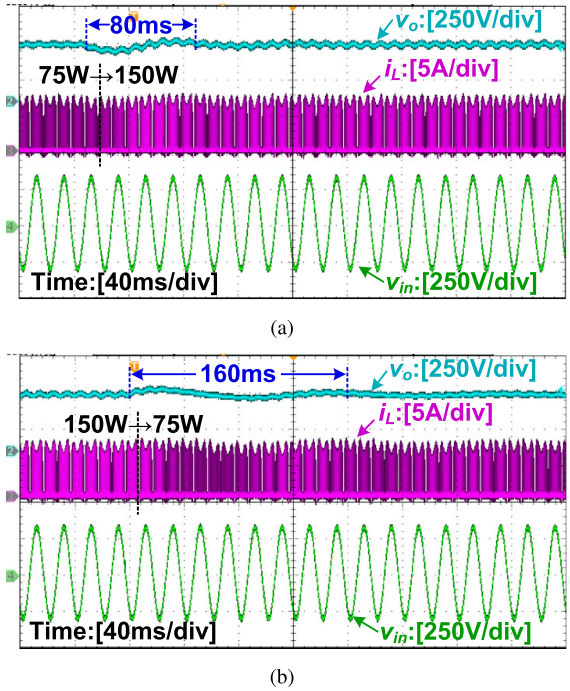

Fig. 22. Transient responses under MEAC control with 220-Vac input when load steps from 75 to 150 W and from 150 to 75 W.

References

[1] J. Mu and L. Liu, "A 12 mV input, 90.8% peak efficiency CRM boost converter with a sub-threshold startup voltage for TEG energy harvesting," *IEEE Trans. Circuits Syst. I*, vol. 65, no. 8, pp. 2631–2640, Aug. 2018.

[2] X. Tang, J. Zeng, K. P. Pun, S. Mai, C. Zhang, and Z. Wang, "Low-cost maximum efficiency tracking method for wireless power transfer systems," *IEEE Trans. Power Electron.*, vol. 33, no. 6, pp. 5317–5329, Jun. 2018.

[3] C.-S. Kwon, W.-K. Choi, and F.-S. Kang, "Maximum efficiency point tracking algorithm for photovoltaic power generating system," in *Proc. 2nd Pacific-Asia Conf. Circuits, Commun., Syst.*, vol. 1, pp. 71–74, 2010.

[4] Y. Lai and M. Yu, "Maximum efficiency point tracking for two-stage server power supply," in *Proc. IEEE 4th Int. Future Energy Electron. Conf.*, 2019, pp. 1–5.

[5] L. Huang, F. Chen, W. Yao, and Z. Lu, "Flexible mode bridgeless boost PFC rectifier with high efficiency over a wide range of input voltage," *IEEE Trans. Power Electron.*, vol. 32, no. 5, pp. 3513–3524, May 2017.

[6] K. Yao, L. Li, H. Tang, C. Mao, and K. Chen, "Optimum boundary inductance control concerning limited PF for a DCM boost PFC converter," *IEEE Trans. Power Electron.*, vol. 35, no. 1, pp. 443–454, Jan. 2020.

[7] Q. Li, K. Yao, J. Song, H. Xu, and Y. Han, "A series diode method of suppressing parasitic oscillation for boost PFC converter operated in discontinuous conduction mode," *IEEE Trans. Power Electron.*, vol. 33, no. 1, pp. 407–424, Jan. 2018.

[8] Y. Chen and Y. Chen, "Line current distortion compensation for DCM/CRM boost PFC converters," *IEEE Trans. Power Electron.*, vol. 31, no. 3, pp. 2026–2038, Mar. 2016.
[9] P. Das, M. Pahlevaninezhad, J. Drobnik, G. Moschopoulos, and P. K. Jain, "A nonlinear controller based on a discrete energy function for an AC/DC boost PFC converter," *IEEE Trans. Power Electron.*, vol. 28, no. 12, pp. 5458–5476, Dec. 2013.
[10] V. M. Lopez, F. J. Azcondo, A. de Castro, and R. Zane, "Universal digital controller for boost CCM power factor correction stages based on current rebuilding concept," *IEEE Trans. Power Electron.*, vol. 29, no. 7, pp. 3818–3829, Jul. 2014.
[11] C. W. Clark, F. Musavi, and W. Eberle, "Digital DCM detection and mixed conduction mode control for boost PFC converters," *IEEE Trans. Power Electron.*, vol. 29, no. 1, pp. 347–355, Jan. 2014.
[12] C. Marxgut, F. Krismer, D. Bortis, and J. W. Kolar, "Ultraflat interleaved triangular current mode (TCM) single-phase PFC rectifier," *IEEE Trans. Power Electron.*, vol. 29, no. 2, pp. 873–882, Feb. 2014.
[13] J. D. Navamani, M. L. Veena, A. Lavanya, and K. Vijayakumar, "Efficiency comparison of quadratic boost DC-DC converter in CCM and DCM," in *Proc. 2nd Int. Conf. Electron. Commun. Syst.*, 2015, pp. 1156–1161.
[14] K. Yao, W. Hu, Q. Li, and J. Lyu, "A novel control scheme of DCM boost PFC converter," *IEEE Trans. Power Electron.*, vol. 30, no. 10, pp. 5605–5615, Oct. 2015.
[15] Q. Huang and A. Q. Huang, "Review of GaN totem-pole bridgeless PFC," *CPSS Trans. Power Electron. Appl.*, vol. 2, no. 3, pp. 187–196, 2017.
[16] X. Ren, Z. Guo, Y. Wu, Z. Zhang, and Q. Chen, "Adaptive LUT-based variable on-time control for CRM boost PFC converters," *IEEE Trans. Power Electron.*, vol. 33, no. 9, pp. 8123–8136, Sep. 2018.
[17] X. Ren, Y. Zhou, Z. Guo, Y. Wu, Z. Zhang, and Q. Chen, "Simple analog-based accurate variable on-time control for critical conduction mode boost power factor correction converters," *IEEE J. Emerg. Sel. Topics Power Electron.*, to be published, doi: 10.1109/JESTPE.2019.2926794.
[18] K. Yao, Y. Wang, J. Guo, and K. Chen, "Critical conduction mode boost PFC converter with fixed switching frequency control," *IEEE Trans. Power Electron.*, vol. 33, no. 8, pp. 6845–6857, Aug. 2018.
[19] N. Swaminathan and N. Lakshminarasamma, "The steady-state DC gain loss model, efficiency model, and the design guidelines for high-power, high-gain, low-input voltage DC-DC converter," *IEEE Trans. Ind. Appl.*, vol. 54, no. 2, pp. 1542–1554, Mar. 2018.
[20] M.-Y. Tsai, T.-J. Liang, and Y.-M. Lin, "Loss analysis and optimized design of DC-DC converter for battery module," in *Proc. IEEE 3rd Int. Future Energy Electron. Conf. ECCE Asia*, Jun. 2017, pp. 692–697.
[21] Y. Guan, Y. Wang, D. Xu, and W. Wang, "A 1 MHz half-bridge resonant DC/DC converter based on GaN FETs and planar magnetics," *IEEE Trans. Power Electron.*, vol. 32, no. 4, pp. 2876–2891, Apr. 2017.
[22] R. Xie, H. Wang, G. Tang, X. Yang, and K. J. Chen, "An analytical model for false turn-on evaluation of high-voltage enhancement-mode GaN transistor in bridge-leg configuration," *IEEE Trans. Power Electron.*, vol. 32, no. 8, pp. 6416–6433, Aug. 2017.

Linkai Li received the B.Eng. and M.S. degrees in automation from the College of Engineering, Nanjing Agriculture University, Nanjing, China, in 2014 and 2017, respectively. He is currently working toward the Ph.D. degree in microelectronics with the School of Optical and Electronic Information, Huazhong University of Science and Technology, Wuhan, China.

His current research interests include the optimal design and digital control of power converters.

Wanyang Wang received the B.Eng. degree in electrical engineering and automation in 2018 from the College of Electrical, Huazhong University of Science and Technology, Wuhan, China, where he is currently working toward the M.S. degree in microelectronics with the School of Optical and Electronic Information.

His current research interests include the optimal design and digital control of power converters.

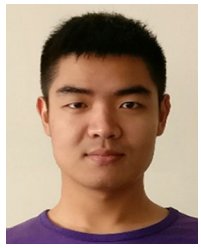

Dian Lyu received the B.Eng. degree in 2016 from the School of Optical and Electronic Information, Huazhong University of Science and Technology, Wuhan, China, where he is currently working toward the Ph.D. degree in microelectronics.

His current research interests include the design and optimization of power electronic systems.

Run Min (Member, IEEE) received the B.Eng. degree from the School of Software and Microelectronics, Northwestern Polytechnical University, Xi'an, China, in 2010, and the Ph.D. degree from the School of Optical and Electronic Information, Huazhong University of Science and Technology (HUST), Wuhan, China, in 2016.

He is currently a Lecturer with HUST. His research interests include modeling, analysis, and control of power electronic systems.

Qiaoling Tong (Member, IEEE) received the B.Eng. and Ph.D. degrees from the School of Optical and Electronic Information, Huazhong University of Science and Technology, Wuhan, China, in 2003 and 2010, respectively.

From 2008 to 2010, he was a Research Scholar with the Department of Electrical Engineering and Computer Science, University of California, Irvine, Irvine, CA, USA. He is currently an Associate Professor with the School of Optical and Electronic Information, Huazhong University of Science and Technology. His current research interests include sensorless control of dc–dc converters and VLSI implementation of intelligent algorithms.

Han Peng (Member, IEEE) received the B.S. degree from Southeast University, Nanjing, China, in 2006, and the Ph.D. degree from Rensselaer Polytechnic Institute, Troy, NY, USA, in 2011, both in electrical engineering.

From 2011 to 2017, she was the Lead Electrical Engineer with the Global Research Center, General Electric Company, Niskayuna, NY, USA. Since 2018, she has been a Professor with the Huazhong University of Science and Technology, Wuhan, China. She has authored/coauthored more than 20 articles in refereed journals and international conference proceedings. She has filed four U.S. patents and two Chinese patents. Her research interests include high-frequency, high power density power management IC design, high-frequency supply modulators and applications of wide bandgap power devices, energy harvesting, communication power, healthcare electronics, more electrical aircraft systems, and electric vehicles.

Dr. Peng has been an Associate Editor for the IEEE TRANSACTIONS ON POWER ELECTRONICS since 2017. She served as the Associate Technical Program Chair for the IEEE 11th Annual Energy Conversion Congress and Exposition in 2019.

Jinchong Yu received the B.Eng. and M.S. degrees from the School of Optical and Electronic Information, Huazhong University of Science and Technology, Wuhan, China, in 2018 and 2020, respectively.

He is currently a Field Application Engineer with Texas Instruments Semiconductor Technologies (Shanghai) Company, Ltd., Shanghai, China. His current research interest includes digital control of power electronic systems.